

Infinite Randomness Phases and Entanglement Entropy of the Disordered Golden Chain

L. Fidkowski and G. Refael

*Department of Physics, Institute for Quantum Information,
California Institute of Technology, MC 114-36, Pasadena, CA 91125*

N. E. Bonesteel

Department of Physics and National High Magnetic Field Laboratory, Florida State University, Tallahassee, FL 32310

J. E. Moore

*Department of Physics, University of California, Berkeley, CA 94720 and
Materials Sciences Division, Lawrence Berkeley National Laboratory, Berkeley, CA 94720*

Topological insulators supporting non-abelian anyonic excitations are at the center of attention as candidates for topological quantum computation. In this paper, we analyze the ground-state properties of disordered non-abelian anyonic chains. The resemblance of fusion rules of non-abelian anyons and real space decimation strongly suggests that disordered chains of such anyons generically exhibit infinite-randomness phases. Concentrating on the disordered golden chain model with nearest-neighbor coupling, we show that Fibonacci anyons with the fusion rule $\tau \otimes \tau = \mathbf{1} \oplus \tau$ exhibit two infinite-randomness phases: a random-singlet phase when all bonds prefer the trivial fusion channel, and a mixed phase which occurs whenever a finite density of bonds prefers the τ fusion channel. Real space RG analysis shows that the random-singlet fixed point is unstable to the mixed fixed point. By analyzing the entanglement entropy of the mixed phase, we find its effective central charge, and find that it *increases* along the RG flow from the random singlet point, thus ruling out a c-theorem for the effective central charge.

I. INTRODUCTION

One of the most interesting frontiers of physics is the behavior of interacting, many body, quantum systems. Such systems are particularly challenging and rich when considered in low dimensionalities, and in the presence of disorder. A common platform for the discussion of collective behavior is a quantum magnet. Already in one dimension, where the behavior of quantum magnets is supposed to be the simplest, surprises emerged: the Haldane gap of integer spin chains^{1,2}, and, more importantly for this work, the random singlet phase^{3,4}. The latter describes the ground state of a disordered spin-1/2 Heisenberg chain, where the spins pair up in and form singlets in a random fashion (fig. 1). Most of the singlets connect near neighbors, but some are very long ranged, and lead to algebraically decaying average correlations. The random singlet phase is the first known example of the infinite-randomness paradigm of 1d random systems. Contrary to the quantum scaling in pure systems, where $1/E \sim L^z$, infinite randomness systems obey the scaling $|\ln E| \sim L^\psi$, and exhibit many other intriguing properties.

Another paradigm for interacting quantum matter is the fractional quantum Hall system. In addition to robust fractionally-charged excitations, Hall bars with electronic densities tuned to special fractions, such as $\nu = 5/2$, and $\nu = 12/5$ are expected to exhibit non-abelian quasi-particles excitations and defects^{5,6}, which may be used to realize a topologically protected qubit^{7,8}, but more importantly, provide an example of a completely

new type of quantum matter. Non-abelian anyons display a remarkable feature: the dimension of the Hilbert space spanned by N non-abelions grows asymptotically as D^N , where D , the quantum dimension of the non-abelion, is irrational. This is a consequence of the so-called fusion rules of the non-abelions. In this paper we will investigate the properties of one-dimensional disordered systems composed of non-abelions, concentrating on the case of the Fibonacci anyons, for which the allowed values of the so-called topological charge can be either 1 or τ .

The investigation of the so-called Fibonacci chain has so far concentrated on the analysis and phases in the translationally invariant case^{9,10}. It turns out that the system is exactly solvable by mapping to an RSOS model, and is described at low energies by a minimal model conformal field theory with central charge $c = \frac{7}{10}$ in the antiferromagnetic case (favoring fusion into the trivial channel) and $c = \frac{4}{5}$ in the ferromagnetic case (favoring fusion into the τ channel). The richness of this example stems from the unique structure of the Hilbert space of a system comprising non-abelian anyons. As we argue below, however, an important insight is that *the construction of the Hilbert state of a random non-abelian chain is analogous to the construction of the ground state and low-lying excitation spectrum of a spin-chain*. Furthermore, contrary to spin chains comprising garden-variety spins, the Hilbert space structure of non-abelian chains guarantees the appearance of an infinite randomness scaling in the presence of disorder. The exotic nature of the non-abelions suggests that the infinite-randomness phases they will exhibit will be new, and perhaps even



FIG. 1: Sample random singlet ground state of a spin-1/2 antiferromagnetic chain. Each line represents a singlet. Singlets form in a random fashion, mostly between nearest neighbors, but occasionally between distant sites giving rise to an average correlation that decays algebraically.

expand our dictionary of infinite-randomness universality classes, currently limited to the permutation symmetric sequence^{11–13}.

Another interesting aspect of infinite-randomness phases is their entanglement entropy. The bipartite entanglement entropy of a pure spin chain at criticality scales logarithmically with its size, and is proportional to the central charge of the conformal field theory describing the critical point^{14–16}. Furthermore, the central charge, and therefore also the entanglement entropy of a pure spin chain, obeys the Zamolodchikov c -theorem: it must decrease along renormalization group flow lines. Random spin chains also have an entropy that scales logarithmically with size, and with a universal coefficient that we identify as an effective central charge^{17–20}. An outstanding question has been whether the c -theorem applies to renormalization group flows between infinite randomness fixed points of the random chains. The evidence so far has been limited, since the overwhelming majority of entanglement entropy calculations were done in the random singlet phase of various systems. The only exception so far has been the entanglement entropy at the critical point between the Haldane phase and the random singlet phase of a spin-1 random antiferromagnet, where the effective central charge indeed decreases along real-space RG flow lines¹⁸. In this paper, we find a real-space RG flow along which the effective central charge increases, thus violating any conjectured c -theorem for flows between strong randomness fixed points.

The first analysis of the random Fibonacci chain²¹ concentrated on the random antiferromagnetic Fibonacci chain. A random singlet phase was found with an effective central charge reflecting the quantum dimension of the Fibonacci anyons: $c_{eff} = \ln \tau$ with $\tau = \frac{1+\sqrt{5}}{2}$ being the golden ratio. In this paper we extend the analysis to the completely disordered Fibonacci chain, which contains both AFM (antiferromagnetic, favoring fusion into a singlet) as well as FM (ferromagnetic, favoring fusion into a τ) bonds - we will refer to it as the *mixed* Fibonacci chain. We find that the random singlet phase is unstable to FM perturbations, and flows to a stable fixed point which, at low energy, is described by an equal mixture of FM and AFM bonds, with identical infinite randomness universal strength distributions. We calculate the entanglement entropy of this new fixed point, and show that it is larger than that in the unstable AFM random-singlet point. We thus have an example of a flow between two infinite randomness fixed points along which the effective

central charge increases.

In the rest of the paper we will describe our analysis of the random Fibonacci chain. In Sec. II we review the real-space renormalization group and the Hilbert space and Hamiltonian of the Fibonacci chain. In Sec. III we define the model, and discuss the decimation rules necessary for a real-space RG analysis. The decimation steps are then used for the calculation of flow equations for the disorder distribution. We use these to derive the phase diagram and investigate the stability of the fixed points found from the flow equations. Sec. IV will describe the entanglement entropy calculation for the random Fibonacci chain. Before concluding, we will discuss the correspondence between the construction of the ground state of a random spin chain, and the construction of the Hilbert space of a chain of non-abelian anyons. This provides the basis for further investigation of other kinds of non-abelian chains, such as the full $SU(2)_k$ sequence.

II. BACKGROUND

A. Real Space Renormalization Group

To find the ground state of disordered spin chains, Ma and Dasgupta introduced the strong disorder real-space renormalization group^{22,23}. The random spin 1/2 Heisenberg model provides the simplest example for this method. The model is given by:

$$H = \sum_i J_{i,i+1} \mathbf{S}_i \cdot \mathbf{S}_{i+1}, \quad (1)$$

where the couplings $J_{i,i+1} > 0$ are positive and randomly distributed. Note that, as far as the Hilbert space is concerned, we have for two neighboring sites

$$\frac{1}{2} \otimes \frac{1}{2} = 0 \oplus 1, \quad (2)$$

and the interactions in the Hamiltonian simply give an energy splitting between the two representations on the right hand side. The procedure now is to pick the largest $J_{i,i+1}$, which effectively truncates the excited triplet and leaves the ground state in a singlet, and do perturbation theory around that state. Quantum fluctuations then induce an effective coupling according to the so-called Ma-Dasgupta rule^{22,23}:

$$J_{i-1,i+2} = \frac{J_{i-1,i} J_{i+1,i+2}}{2J_{i,i+1}} \quad (3)$$

So sites i and $i+1$ are decimated and replaced with an effective interaction between $i-1$ and $i+2$. Iteration of this procedure produces bonds on all length scales. This is the random singlet ground state.

A quantitative description is obtained by tracking the RG flow of the coupling distribution. It is useful to employ logarithmic couplings³:

$$\beta_{i,i+1} = \ln \frac{\Omega}{J_{i,i+1}} \quad (4)$$

where $\Omega = \max_i J_{i,i+1}$. In these variables the Ma-Dasgupta rule (3) reads

$$\beta_{i-1,i+2} = \beta_{i-1,i} + \beta_{i+1,i+2} \quad (5)$$

(up to an additive constant of $\ln 2$ which can be safely neglected). As the couplings get decimated Ω decreases. It is convenient to define the RG flow parameter as

$$\Gamma = \ln \frac{\Omega_0}{\Omega} \quad (6)$$

where Ω_0 is the maximal coupling of the bare Hamiltonian. Let $P_\Gamma(\beta)$ be the distribution of couplings. We can derive a flow equation for $P_\Gamma(\beta)$ by decimating the couplings in the infinitesimal interval $\beta = [0, d\Gamma]$ and seeing how their probabilistic weight is redistributed. We obtain

$$\begin{aligned} \frac{d}{d\Gamma} P_\Gamma(\beta) &= \frac{\partial P_\Gamma}{\partial \beta} + \\ P(0) \int_0^\infty d\beta_1 \int_0^\infty d\beta_2 \delta(\beta - \beta_1 - \beta) P_\Gamma(\beta_1) P_\Gamma(\beta_2) \end{aligned} \quad (7)$$

The first term comes from the overall change of scale, and the second from the Ma-Dasgupta rule. These equations have a solution

$$P_\Gamma(\beta) = \frac{1}{\Gamma} e^{-\beta/\Gamma} \quad (8)$$

which is an attractive fixed point to essentially all physical initial configurations. This solution permits us to read off features of the random singlet phase; for example one can with a little more work derive the energy-length scaling relation:

$$L^{1/2} \sim \Gamma = \ln(1/E). \quad (9)$$

which thus has the exponent:

$$\psi = 1/2. \quad (10)$$

B. Hilbert Space and Hamiltonian of the Fibonacci Chain

We now construct the Hilbert space and Hamiltonian of the Fibonacci chain. The system is modeled as a chain of non-abelian anyons carrying the non-trivial topological charge τ . Heuristically, we want the property that

$$\tau \otimes \tau = 1 \oplus \tau \quad (11)$$

which states that the Hilbert space of two neighboring τ 's is the direct sum of a trivial component and another copy of τ . This unusual property immediately prevents us from describing the Hilbert space as a tensor product of local degrees of freedom. Indeed, a naive interpretation of the tensor product in (11) would give the dimension of the space τ to be the golden ratio, an irrational number. This problem is resolved by the adoption of the

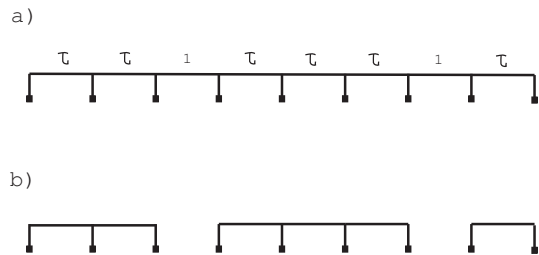


FIG. 2: a) A state in the Hilbert space: the labels 1 and τ specify the total topological charge of all the sites to the left (or equivalently right) of the bond, with the fusion rules obeyed at each trivalent node b) The same state in graph notation - we only draw the τ 's.

machinery of *truncated* tensor products of representations of $SU(2)$ at level k , but rather than developing it here we instead give two elementary constructions of the Hilbert space. We note, however, the analogy between (2) and (11); indeed the Hamiltonian, defined below, will simply yield an energy splitting between the two representations on the right hand side of (11).

The simplest way to construct the Hilbert space is to define basis states by labeling each link between two τ 's with a 1 or τ , with the constraint that one is not allowed to have two consecutive 1's - fig. 2(a). The dimension D_N of the Hilbert space for N sites then follows the Fibonacci recursion

$$D_N = D_{N-1} + D_{N-2} \quad (12)$$

which is solved by $D_N \sim \tau^N$. Thus there are $\tau \simeq 1.618$ "degrees of freedom" on each site (note: we use τ to denote the nontrivial topological charge and the value of the golden mean, as well as the corresponding representation of $SU(2)_k$ where appropriate).

While this link description of the Hilbert space is most convenient computationally, there is an equivalent but more abstract one that is useful in defining the Hamiltonian and carrying out the real space RG procedure. In this abstract description the Hilbert space is defined as the set of all trivalent graphs with endpoints at the N nodes, modulo the F -matrix relations - see fig.3 - where the F matrix is

$$F = \begin{bmatrix} \tau^{-1} & \tau^{-1/2} \\ \tau^{-1/2} & -\tau^{-1} \end{bmatrix} \quad (13)$$

The edges of the graph represent nontrivial topological charge τ and trivalent vertices represent the fusion of two τ 's into another τ . To relate this graphical picture to the link basis, note that the link basis states can be viewed as trivalent graphs, as in fig. 2(b), and any other trivalent graph can be reduced to a superposition of these using F -matrix moves (for example, see fig. 4). The inner product of two graphs is defined by reflecting one of the graphs and concatenating it with the other along the N nodes.

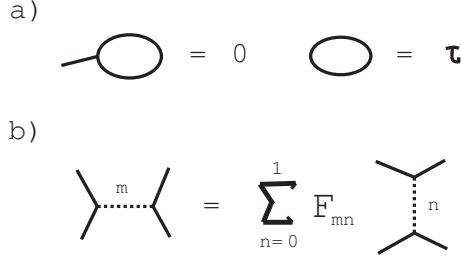


FIG. 3: The F -matrix relations. a) graphs that can be disconnected by cutting one edge are equal to 0 (the no tadpole condition) and disconnected loops are worth τ . b) local reconnection rules are given by the F -matrix, defined in the text. Here m and n are binary variables equal to either τ or 1 - i.e., the link is either there or not

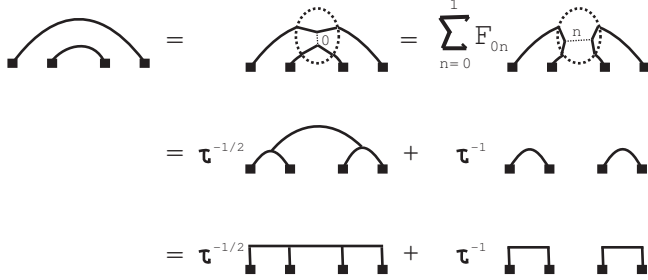


FIG. 4: The trivalent graph on the left hand side expressed in terms of the link basis.

We now define the Hamiltonian. There are two kinds of nearest neighbor interactions we consider: we can either project onto total topological charge τ of the pair, in which case we refer to the interaction as ferromagnetic (F), or onto the trivial charge 1 - this interaction is antiferromagnetic (A). The F and A designations are by analogy with the spin 1/2 case, where antiferromagnetic interactions favor a singlet, which has trivial spin, and ferromagnetic interactions favor non-zero total spin

$$\mathcal{H} = \sum J_i (1 - P_i^{\Sigma_i}), \quad (14)$$

where for each site J_i is a positive random number with a given distribution, and $\Sigma_i = A$ for the Hamiltonian describing the AFM fixed point, while $\Sigma_i = F$, A at random for the Hamiltonian describing the mixed FM/AFM fixed point. Here $P_i^{F/A}$ are the projectors onto the ferromagnetic and antiferromagnetic sectors of the pairs of sites. These projection operators are defined graphically in fig. 5. They can also be viewed in the link basis if we apply F -matrix rules to decompose the result of the concatenations in fig. 5.

As an illustration of the complicated nature of the Hilbert space, we analyze the “rainbow” state that arises in the entanglement entropy calculation for the AFM chain²¹ - see fig. 6 (a). If we assume the partition bond (i.e., the bond that divides the system into two subsystems) to lie in the middle of the chain, then this state

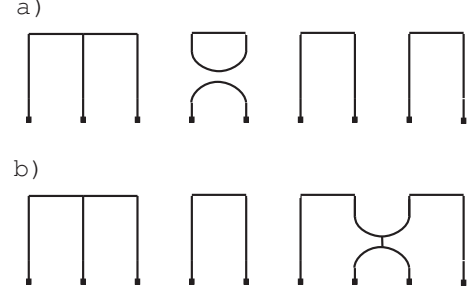


FIG. 5: a) Projection operator P_i^A on a pair of sites. b) Projection operator P_i^F on a different pair of sites.

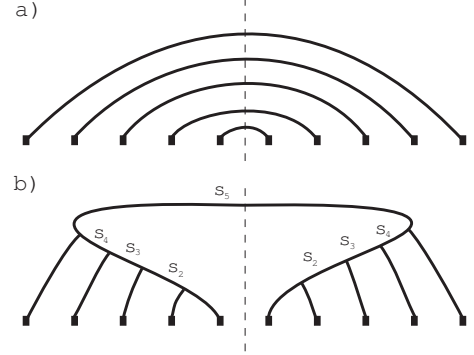


FIG. 6: A rainbow diagram. The partition bond is in the middle.

turns out to be quite entangled. We will be more precise later, but the idea is that to compute the entanglement entropy, we want to use F -matrix moves to write the state as a superposition of states shown in fig. 6 (b). This way we push all the nontrivial parts of the graph into one of the two halves, and the entanglement can be read off from the coefficients of the new states. Carrying this out, Ref. 21 showed that for large number N of singlets, the entropy is asymptotically $N \log_2 \tau$. Thus the asymptotic contribution of each singlet is $\log_2 \tau$. Note, however, that when N is small, there are deviations from this form. In particular, when $N = 1$, so that we have only one τ anyon in each half, the Hilbert space has only one state and so the state counting entropy is 0. These sorts of subtleties will be treated carefully when we do our entropy calculation for the mixed FM/AFM fixed point.

III. INFINITE RANDOMNESS FIXED POINTS OF THE GOLDEN CHAINS

A. Ma-Dasgupta decimation rules

The graphical description of the Hilbert space in terms of trivalent graphs shows how the real space RG method can be generalized to the case of the mixed Fibonacci chain, containing both FM and AFM interactions. As

before one first picks the largest coupling J_i in eqn. (14) and assumes that it localizes a state on i and $i+1$ with total topological charge either 1 or τ , depending on whether the interaction is AFM or FM. Graphically this localization is just a restriction to graphs that have a singlet spanning the two sites (AFM case) or graphs that have the two τ 's at i and $i+1$ fuse into another τ (FM case). Again the state of the two sites is perturbed by the other two bonds connecting these sites to the rest of the chain.

To study the effect of this perturbation consider the Hamiltonian (14) acting on four tau particles with site labels 1 through 4. Using the fact that $P_i^F = 1 - P_i^A$ this Hamiltonian can, up to an irrelevant constant, be taken to be

$$H = -J_1 P_1^A - J_2 P_2^A - J_3 P_3^A, \quad (15)$$

where now the sign of a given J_i , connecting particles at sites i and $i+1$, can be positive or negative, corresponding to AFM or FM bonds, respectively. We then assume that J_2 is the highest energy bond, with $|J_2| \gg |J_1|, |J_3|$, and write (15) as $H = H_0 + H'$ where $H_0 = -J_2 P_2^A$ is the “unperturbed” Hamiltonian and $H' = -J_1 P_1^A - J_3 P_3^A$ is the perturbation.

First consider the case of decimating an AFM bond for which $J_2 > 0$. The two degenerate ground states of H_0 will have a singlet connecting particles 2 and 3 (i.e., these two particles will have total topological charge 1) while particles 1 and 4 can combine to either have topological charge 1 or τ . We denote these two unperturbed states $|\psi_1\rangle$ and $|\psi_\tau\rangle$. Since the total topological charge of the four particles is a “good” quantum number, the perturbation H' will lead to an energy splitting, J_{eff} , between the state of these four particles with total topological charge 1 and the state with total topological charge τ . This energy splitting can then be described by a new Hamiltonian $H_{eff} = -J_{eff} P_1^A$, where now P_1^A acts on particles 1 and 4. It is straightforward to compute J_{eff} using second order perturbation theory with the result,

$$J_{eff} = \frac{|\langle\psi_1|H'P_2^F H'|\psi_1\rangle|}{J_2} - \frac{|\langle\psi_\tau|H'P_2^F H'|\psi_\tau\rangle|}{J_2}. \quad (16)$$

In this expression the FM projection operator P^F projects $H'|\psi_{1,\tau}\rangle$ onto the excited Hilbert space of the unperturbed Hamiltonian H_0 with energy J_2 above the ground state.

Using the techniques described in the previous section the matrix elements appearing in (16) can be evaluated to find

$$\begin{aligned} |\langle\psi_1|H'P_2^F H'|\psi_1\rangle|^2 &= (J_1 + J_3)^2 \frac{1}{\tau^2} \\ &- \left((J_1 + J_3) \frac{1}{\tau^2} \right)^2, \end{aligned} \quad (17)$$

$$\begin{aligned} |\langle\psi_\tau|H'P_2^F H'|\psi_\tau\rangle|^2 &= (J_1^2 + J_3^2) \frac{1}{\tau^2} \\ &- \left((J_1 + J_3) \frac{1}{\tau^2} \right)^2. \end{aligned} \quad (18)$$

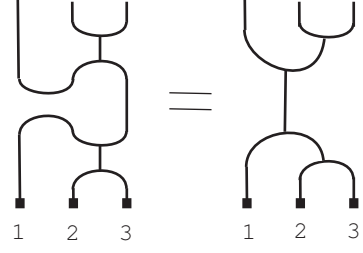


FIG. 7: Particles 2 and 3 are decimated ferromagnetically. The effect on an AFM projection acting on 1 and 2 is simply to turn it into an FM projection. For an AFM projector (FM projector) there is a numerical factor associated to the graphical representation above of τ^{-1} ($\tau^{-1/2}$). Combining these, we get $\tau^{-1}(\tau^{-1/2})^2 = \tau^{-2}$, of which $\tau^{-1/2}$ gets absorbed in the normalization for the new FM projector and another $\tau^{-1/2}$ goes into the normalization of the wavefunction, leaving τ^{-1} . Thus P^A on sites 1 and 2 turns into $\frac{1}{\tau}P^F$. A similar graphical argument shows that P^F turns into $\frac{1}{\tau}P^A$.

It then follows that

$$J_{eff} = \frac{2}{\tau^2} \frac{J_1 J_3}{J_2}. \quad (19)$$

Thus we see that when an AFM bond is decimated the usual Ma-Dasgupta rule holds. The value of the coefficient $2/\tau^2$ is not significant except for the fact that, because it is less than 1, J_{eff} will always be less than J_2 . As for the usual Ma-Dasgupta rule, the resulting interaction will be AFM if J_1 and J_3 have the same sign, and FM if J_1 and J_3 have opposite signs.

Next consider the case of a FM bond for which $J_2 < 0$ in (15). In this case the two tau particles connected by J_2 fuse to form a cluster with topological charge τ . The tau particles on either side of this cluster will then interact with it, but with modified interaction strengths \tilde{J}_1 and \tilde{J}_3 .

To compute these modified interactions, consider particle 1, which is coupled to the newly formed cluster through the “bare” interaction J_1 . To see the effect of the decimation on any operator O on the pair of particles 1 and 2, we simply project this operator down to the decimated subspace: $O_{\text{new}} = P^F O P^F$ where P^F acts on particles 2 and 3. Composing the operators graphically in fig. 7 we see that P^F turns into P^A and vice versa, with an extra factor of $1/\tau$.

Another way to see this is as follows. There are two possible states for the tau particle at site 1 and the τ cluster formed by particles 2 and 3 — the total topological charge of all three particles can be either 1 or τ . Again we denote these two states $|\psi_1\rangle$ and $|\psi_\tau\rangle$. In this case the effective interaction can be computed using first order perturbation theory in $H' = -J_1 P_1^A$ with the result

$$\tilde{J}_1 = \langle\psi_1|J_1 P_1^A|\psi_1\rangle - \langle\psi_\tau|J_1 P_1^A|\psi_\tau\rangle. \quad (20)$$

The calculation of these matrix elements is again

straightforward and we find that

$$\langle \psi_1 | P_1^A | \psi_1 \rangle = 0, \quad (21)$$

$$\langle \psi_\tau | P_1^A | \psi_\tau \rangle = \frac{1}{\tau}. \quad (22)$$

Thus we obtain

$$\tilde{J}_1 = -\frac{1}{\tau} J_1. \quad (23)$$

The same argument implies that $\tilde{J}_3 = -\frac{1}{\tau} J_3$. The essential feature here is that when a FM bond is decimated the sign of the effective interaction with the neighboring tau particles is flipped — FM bonds become AFM bonds and vice versa. In addition there is numerical reduction of the bond strength by a factor of $1/\tau$. However, as above, the value of this coefficient is not important for determining the fixed-point behavior of the model — the only important fact is that it is less than 1 so we are guaranteed that $|\tilde{J}_1| < |J_2|$.

The two above results for decimation of strong bonds constitute the strong-randomness RG rules of the mixed random Fibonacci chain. In the following we will derive the RG flow equations for this case and show that it has non-trivial fixed points.

B. Flow equations for the Fibonacci chain

In order to explore the phase diagram of the golden chain, we must first turn the Ma-Dasgupta rules for the decimation of ferromagnetic (FM) and antiferromagnetic (AFM) bonds, eq. (19), to flow equations. This goal was partially achieved in Ref. 21 for a golden chain which contains only AFM bonds. As we shall see, including FM bonds in this analysis reveals a new fixed point, where the number of FM and AFM bonds is the same.

We begin our analysis by introducing the logarithmic

notation for bond strengths:

$$\beta_i = \ln \frac{\Omega}{|J_i|} \quad (24)$$

where $\Omega = \max_i \{|J_i|\}$ so that the AFM Ma-Dasgupta rule (19) reads $\beta_{eff} = \beta_{i-1} + \beta_{i+1} - \ln C$. Note that while the β_i 's carry the information about bond strengths, they do not specify whether a bond is FM and AFM, and $\beta_i \geq 0$. Let us next define the coupling distributions for the AFM (positive J 's) and FM bonds (negative J 's), respectively:

$$P(\beta), N(\beta). \quad (25)$$

The probability of a bond to be AFM (A), or FM (F) are thus

$$p_A = \int_0^\infty d\beta P(\beta) \quad (26)$$

$$p_F = 1 - p_A = \int_0^\infty d\beta N(\beta).$$

In addition, we define $\Gamma = \ln \frac{\Omega}{\Omega_0}$ to be the logarithmic RG flow parameter. Its initial value is a non-universal constant of order 1, and as the RG progresses, it flows to ∞ .

The flow equations for $P(\beta)$ and $N(\beta)$ are derived in analogous fashion to those of the distributions in the spin 1/2 problem³. Roughly speaking, the terms appearing in the two flow equations are the result of: (a) rescaling of the UV cutoff Ω , (b) decimation of an AFM bond, (c) decimation of a FM bond. Below we will write the flow equations with each term followed by an explanation or a diagram of the decimation step giving rise to it. In the graphical representation on the right column below, A and F represent antiferromagnetic and ferromagnetic bonds respectively, and the bond decimated is represented by the bold letter with the hat. Let us start with the flow of the AFM bond distribution:

$$\begin{aligned} \frac{dP}{d\Gamma} = & \frac{\partial P}{\partial \beta} & (\text{cutoff rescaling}) \\ & + P(0) \int_0^\infty d\beta_1 \int_0^\infty d\beta_2 \delta(\beta_1 + \beta_2 - \beta) P(\beta_1) P(\beta_2) & \bullet A \bullet \hat{A} \bullet A \bullet \Rightarrow \bullet A \bullet \\ & + P(0) \int_0^\infty d\beta_1 \int_0^\infty d\beta_2 \delta(\beta_1 + \beta_2 - \beta) N(\beta_1) N(\beta_2) & \bullet F \bullet \hat{A} \bullet F \bullet \Rightarrow \bullet A \bullet \\ & - 2P(0)P & (\text{neighbor removal in AFM decimation}) \\ & + 2N(0)N & \bullet F \bullet \hat{F} \bullet F \bullet \Rightarrow \bullet A \bullet A \bullet \\ & - 2N(0)P & (\text{removal of neighboring AFM in FM decimation}) \\ & + (2P(0) + N(0))P \end{aligned} \quad (27)$$

The last term feeds back the probability of bonds lost due to an AFM decimation, which removes a net of two bonds $[2P(0)]$, and due to a FM decimation, which removes a single bond $[N(0)]$.

Carrying out the analogous considerations for the FM bond distribution:

$$\begin{aligned}
& +2P(0) \int_0^\infty d\beta_1 \int_0^\infty d\beta_2 \delta(\beta_1 + \beta_2 - \beta) N(\beta_1) P(\beta_2) && \text{(cutoff rescaling)} \\
& && \bullet F \bullet \hat{\mathbf{A}} \bullet A \bullet \Rightarrow \bullet F \bullet \\
& -2P(0)N && \text{(neighbor removal in AFM decimation)} \\
& +2N(0)P && \bullet A \bullet \hat{\mathbf{F}} \bullet A \bullet \Rightarrow \bullet F \bullet F \bullet \\
& -2N(0)N && \text{(removal of neighboring FM in FM decimation)} \\
& +(2P(0) + N(0))N.
\end{aligned} \tag{28}$$

Once more, the last line makes sure that probability is conserved.

Adding up all the above terms yields the following concise flow equations:

$$\begin{aligned}
\frac{dP}{d\Gamma} &= \frac{\partial P}{\partial \beta} + P(0) (P \otimes P + N \otimes N) + 2N(0)N(\beta) - N(0)P(\beta) \\
\frac{dN}{d\Gamma} &= \frac{\partial N}{\partial \beta} + 2P(0)N \otimes P - N(0)N(\beta) + 2N(0)P(\beta),
\end{aligned} \tag{29}$$

where we also introduce the notation:

$$F \otimes G = \int_0^\infty dx_1 \int_0^\infty dx_2 \delta(x - x_1 - x_2) F(x_1) G(x_2). \tag{30}$$

C. Fixed points of the real-space RG

From the flow equations, Eqs. (29), we can find the fixed points of the golden chain. These appear as attractors of the integro-differential equations. To find them, we first note that we can eliminate Γ by guessing a scale-invariant solution³:

$$P_\Gamma(\beta) = \frac{1}{\Gamma} p(\beta/\Gamma), \quad N_\Gamma(\beta) = \frac{1}{\Gamma} n(\beta/\Gamma). \tag{31}$$

Substituting this scaling ansatz gives:

$$\begin{aligned}
-p &= (1+x)p' + p_0(p \otimes p + n \otimes n) + 2n_0n - n_0p \\
-n &= (1+x)n' + 2p_0n \otimes p + 2n_0p - n_0n.
\end{aligned} \tag{32}$$

Furthermore, the convolution hidden by the \otimes sign compels us to assume an exponential form for the unknown functions $n(x)$, $p(x)$:

$$p(x) = p_0 e^{-\gamma x} \quad n(x) = n_0 e^{-\gamma x}. \tag{33}$$

This ansatz reduces the integro-differential equations, Eqs. (29), to a set of three simple algebraic equations:

$$\begin{aligned}
\gamma &= p_0^2 + n_0^2 \\
n_0(\gamma - 2p_0^2) &= 0 \\
n_0 + p_0 &= \gamma.
\end{aligned} \tag{34}$$

The exponential ansatz and the resulting Eqs. (34) reveal two fixed-point solutions. A first solution of (34) corresponds to the pure AFM fixed point:

$$n_0 = 0. \quad p_0 = \gamma = 1. \tag{35}$$

This is the random singlet phase discussed in Ref. 21. A new fixed point, however, is found by allowing n_0 to be nonzero:

$$\gamma = 2, \quad p_0 = n_0 = 1. \tag{36}$$

This fixed point has an equal proportion of FM and AFM bonds, and although it is an infinite-randomness fixed point, it is not a random-singlet point. Translating back to the original variables, the coupling distributions are:

$$N(\beta) = P(\beta) = \frac{1}{\Gamma} e^{-2\beta/\Gamma}. \tag{37}$$

While $\gamma = 2$ is one universal critical exponent describing the universality class of the mixed FM/AFM phase, another critical exponent is ψ , which describes the energy-length scaling:

$$\ln \frac{1}{E} \sim L^\psi. \tag{38}$$

This is equivalent to:

$$n \sim \frac{1}{\Gamma^{1/\psi}}, \tag{39}$$

with $n \sim 1/L$ here being the density of undecimated sites.

To obtain ψ , let us compute the density of free sites at the energy scale Γ . A FM bond decimation eliminates one site, while an AFM decimation eliminates two sites. This implies that the total density of undecimated sites obeys:

$$\frac{1}{n} \frac{dn}{d\Gamma} = -N(0) - 2P(0) = -3 \frac{1}{\Gamma} \tag{40}$$

and therefore:

$$n = \frac{n_I}{\Gamma^3}, \quad (41)$$

which corresponds to the infinite randomness critical exponent:

$$\psi = 1/3. \quad (42)$$

From ψ and γ of the mixed FM/AFM fixed point of the Fibonacci random chain, we see that it is in the same universality class as the fixed point separating the gapped Haldane-phase and the random singlet phase of the $S = 1$ random chain.

D. Stability of the phases

In the previous section we found the two fixed points of the random golden chain. In order to construct its phase diagram, however, we must also study the stability of these fixed points. As it turns out, the random-singlet phase is actually *unstable*, and flows to the mixed FM/AFM fixed point.

Let us begin our analysis with the mixed FM/AFM phase. Assume a perturbation that breaks the balance between FM and AFM bonds:

$$N(\beta) = (1 - \delta)\frac{1}{\Gamma}e^{-2\beta/\Gamma}, \quad P(\beta) = (1 + \delta)\frac{1}{\Gamma}e^{-2\beta/\Gamma}. \quad (43)$$

Substituting in Eqs. (29) very readily yields:

$$\Gamma \frac{d\delta}{d\Gamma} = -5\delta, \quad (44)$$

indicating stability with respect to FM/AFM imbalance.

By establishing the stability of the mixed phase, we essentially doom the random singlet phase to be unstable. Complementing the analysis, however, near the AFM random singlet fixed point, we assume:

$$N(\beta) = \delta\frac{1}{\Gamma}e^{-\beta/\Gamma} \quad P(\beta) = (1 - \delta)\frac{1}{\Gamma}e^{-\beta/\Gamma}. \quad (45)$$

Again, substitution in Eqs. (29) yield:

$$\Gamma \frac{d\delta}{d\Gamma} = 2\delta, \quad (46)$$

which means that FM bonds are a relevant perturbation. In addition, we find that the cross-over exponent is:

$$\chi = 2. \quad (47)$$

These results allow us to draw the flow diagram, Fig. 8. Thus the golden chain is in the AFM random-singlet phase when it initially consists of only AFM bonds. On the other hand, any finite density of FM bonds leads to the mixed FM/AFM fixed point.

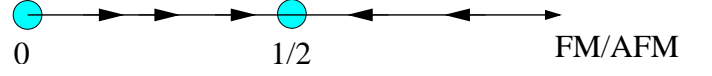


FIG. 8: Flow diagram for the mixed Fibonacci chain. Two fixed points exist. The AFM fixed point is unstable with respect to introduction of FM bonds. A stable fixed point exists at the symmetric FM-AFM point.

IV. ENTANGLEMENT ENTROPY AT THE SYMMETRIC FM-AFM POINT

A. Overview of the calculation

In this section we calculate the asymptotic scaling of the block entanglement entropy of the disordered Fibonacci chain, that is, the entanglement entropy between a region of L consecutive sites and its complement. Because of the non-local nature of the Hilbert space, some subtleties arise. Let us first define entanglement entropy, and then motivate our definition. Given two regions A and B , we have, as illustrated in fig. 9, superselection sectors for the topological charge, with the total Hilbert space

$$H = H_A^0 \otimes H_B^0 \oplus H_A^1 \otimes H_B^1. \quad (48)$$

Here the superselection sectors H_A^i and H_B^i can formally be thought of as n -point disk spaces. Given a state $\psi \in H$ we decompose it according to (48) as $\psi = \psi^0 + \psi^1$. Each of these has a Schmidt decomposition

$$\psi^i = \sum_j \lambda_j^i \eta_j^i \otimes \chi_j^i \quad (49)$$

where the states $\eta_j^i \otimes \chi_j^i$ have unit norm in H . We now define the entanglement entropy in the usual way, as

$$S = - \sum_{i,j} \lambda_j^i \log_2 \lambda_j^i. \quad (50)$$

To motivate this definition we note that it is equivalent to the standard definition of entanglement entropy when we implement the fusion rule constraints via large energy penalties E in the Hamiltonian. Specifically, working in the link basis for convenience, we enlarge the Hilbert space to a space H' that allows all link configurations, with terms added to the Hamiltonian to penalize violations of the fusion rules. We extend the inner product and Hamiltonian to H' in the simplest way possible - say, by extending the Hamiltonian to be kE times the identity on the space V_k of configurations with k violations of the fusion rules, and taking the inner product such that V_k is orthogonal to V_l for $k \neq l$. The new hamiltonian is Hermitian on H' , preserves $H \subset H'$, and reduces to the original Hamiltonian on H . For E much larger than the ground state energy in the original problem, the ground state and all low lying states in the new problem are the same as those in the original one. The upshot is that

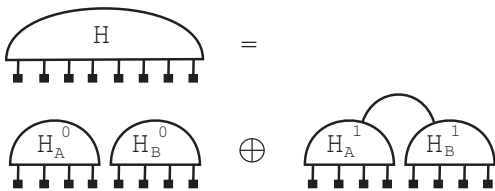


FIG. 9: Decomposition of the total Hilbert space into superselection sectors.

H' now has a tensor product decomposition, and entanglement entropy can be defined in the conventional way (some care must be taken in normalizing inner products on the sub-system Hilbert spaces). This conventional definition for states in $H \subset H'$ coincides with ours above. We also note that this is how entanglement entropy was defined in the numerical algorithm of Ref. 9, which recovered the central charges $c = 4/5, 7/10$ in the uniform case of the golden chain.

The calculation of the entanglement entropy for the Fibonacci chain proceeds along the same lines as previous calculations of the entropy. To gain orientation for the calculation we will shortly pursue, let us review the entanglement entropy calculation for the simplest instance of an infinite randomness fixed point, the spin $1/2$ Heisenberg model¹⁷. There, the basic idea is to count the number of singlets formed over a boundary of the interval, up to a cutoff size L (energy-length scaling turns this into a cutoff in Γ). Each singlet contributes 1 to the entanglement entropy. Real space RG analysis shows that the number of singlets is proportional to $\log \Gamma \sim \log L$, so we obtain logarithmic scaling of the block entanglement entropy. It turns out that this logarithmic scaling persists in the disordered fibonacci chain, but obtaining the coefficient in front of the log is considerably more difficult. For one thing, we already saw earlier (discussion preceding fig. 6) that even in the AFM fixed point, obtaining the entanglement entropy required using F -moves to change to a more convenient basis.

Obtaining the entropy in the mixed fixed point of the Fibonacci chain is even more difficult, because the ground state now contains not just singlets but also complicated tree-like structures, since two τ 's can fuse into another τ , and not just to a singlet. The problem, however, is still tractable, although instead of looking at the RG time between successive singlets, we must now look at RG times between consecutive AFM decimations, and the tree-like structures that form between them (fig. 11a). Just as each singlet in the AFM case contributed asymptotically $\log_2 \tau$ in the case of many singlets, we will find a similar simplification in the mixed case for a large number of AFM decimations - each tree-like structure will asymptotically contribute some amount to the entropy. The RG process will average over all trees, so we will have some average contribution $\langle S_{\text{tree}} \rangle$ to the entanglement entropy. To get the dependence on the block length L , we first use energy-length scaling to relate L to the RG flow variables: $\frac{1}{3} \ln L \sim -\ln \Gamma \sim l$. We show in the next sub-

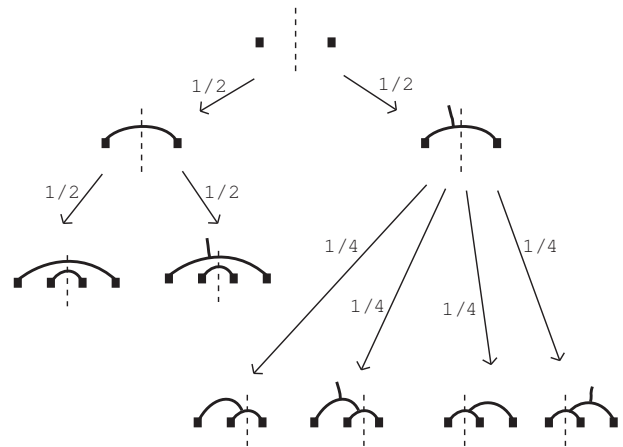


FIG. 10: RG history near the partition bond (represented by the dashed vertical line). The partition bond is at some point decimated, with equal probabilities of having an AFM and FM decimation. In the case of an AFM decimation, we get another partition bond, which will at some point be decimated by an AFM or FM decimation, again with equal probability. In the case of an FM decimation, however, we produce a partition site, which can decimate, either via AFM or FM decimation, with either the site to its left or the site to its right. All four of these possibilities are equally likely. Carried out further, this process will generate complicated tree-like structures. Note that we have ignored decimations that do not involve the partition bond or partition site

section that AFM decimations occur with period $3/2$ in l . Thus for a block of size L , we have $n \sim \frac{2}{3}l \sim \frac{2}{9} \ln L$ AFM decimations separating tree-like structures straddling each endpoint of the block, which gives a contribution of

$$\frac{4}{9} < S_{\text{tree}} > \ln L. \quad (51)$$

We will see that there will also be another contribution to the entanglement entropy, coming from the residual singlets left straddling the endpoints after the tree-like structures have been resolved. We will compute this "rainbow" contribution carefully later in this section, but first we turn to calculating the RG times between the various decimations.

B. RG times between decimations

A pictorial representation of the RG process is given in fig. 10. We see that eventually a ground state of the form shown in fig. 11 is generated. To quantitatively understand real space RG, we will need to compute the (log) of the RG times between various types of decimations.

Now, in the simple case of the spin $1/2$ Heisenberg model, one is interested in (log of) the RG time between successive decimations of the partition bond - the bond

through which the boundary of the region passes. After each decimation of the partition bond, the coupling distribution at the bond is different than the average distribution in the chain. Nevertheless, it is independent of the other surviving bonds¹⁷, and in that sense, it 'resets'. Thus the RG time duration between successive decimations obeys a Poisson distribution characterized by one number, the average of the log of the RG time between successive decimations. No history dependence of this number appears for the antiferromagnet.

Our mixed Fibonacci case is more complicated due to the presence of both FM and AFM decimations. Here we must consider all possible histories of FM and AFM decimations, as illustrated in fig. 10, and compute probabilities for each. Nevertheless, the Fibonacci chain has several simplifying factors which make the problem more tractable. First, as in the case of the spin-1 Heisenberg chain calculation, once the partition bond undergoes an AFM decimation, the resulting distribution of the coupling across the partition bond is 'reset', and is independent of the chain's history. Second, the distribution of bond strengths is always symmetric with respect to exchange of FM and AFM couplings. It turns out that it is characterized by just two numbers, the time between an AFM decimation and the next decimation (equally likely to be FM and AFM by symmetry), and the time between a FM decimation and the next one (again equally likely to be FM and AFM).

To see this, we notice that the joint probability distribution of all the bonds takes one of two forms, depending on whether we've just had a FM or AFM decimation. Immediately following an AFM decimation, we have an independent distribution for all bonds, with the partition bond having distribution

$$Q(\beta) = \frac{2\beta}{\Gamma^2} e^{-2\beta/\Gamma} \quad (52)$$

and all the other bonds following $P(\beta) = \frac{1}{\Gamma} e^{-\beta/\Gamma}$. FM decimations are even simpler: after an FM decimation, all the bonds follow $P(\beta) = \frac{1}{\Gamma} e^{-\beta/\Gamma}$. The surrounding bonds do get changed from AFM to FM and vice versa, but because they are equally likely to be one or the other at the mixed fixed point (i.e., the distribution is symmetric with respect to the interchange) there is no net effect. One can verify these observations by noting, as in 17, that under RG evolution following an AFM decimation the distribution retains its form, with Q changing in a complicated way and P evolving as its explicit dependence on Γ dictates. In fact, in much the same way as is done in Ref. 17 we can derive an equation for the RG evolution of Q :

$$\begin{aligned} \frac{dQ_\Gamma(\beta)}{d\Gamma} &= Q'_\Gamma(\beta) - \frac{2}{\Gamma} Q_\Gamma(\beta) + \\ &\frac{4}{\Gamma} \int d\beta_1 d\beta_2 \delta(\beta - \beta_1 - \beta_2) P_\Gamma(\beta_1) Q_\Gamma(\beta_2). \end{aligned} \quad (53)$$

We solve it by making the ansatz

$$Q_\Gamma = \left(a + b \frac{2\beta}{\Gamma}\right) \frac{1}{\Gamma} e^{-2\beta/\Gamma}, \quad (54)$$

with a and b functions of Γ . Let $l = \ln \frac{\Gamma}{\Gamma_0}$, where Γ_0 is the RG time when the AFM decimation occurred. The initial conditions at $l = 0$ are then $a = 0, b = 1$. Plugging the ansatz into (53) then yields

$$\begin{aligned} \frac{da}{dl} &= -3a + 2b, \\ \frac{db}{dl} &= a - 2b. \end{aligned} \quad (55)$$

The solution is

$$\begin{aligned} a &= \frac{2}{3} (e^{-l} - e^{-4l}), \\ b &= \frac{1}{3} (2e^{-l} + e^{-4l}). \end{aligned} \quad (56)$$

To extract the expected value $\langle l \rangle$ until the next decimation, note that the probability p that another decimation has not occurred by RG time $\Gamma > \Gamma_0$ is simply

$$p_\Gamma = \int_0^\infty d\beta Q_\Gamma(\beta) = a_\Gamma + b_\Gamma. \quad (57)$$

The expected value of l at the next decimation is then

$$\begin{aligned} \langle l \rangle &= - \int_0^\infty l dp_\Gamma = 2 \int_0^\infty a l dl \\ &= \frac{4}{3} \int_0^\infty (e^{-l} - e^{-4l}) dl = \frac{15}{12}. \end{aligned} \quad (58)$$

Notice that $\langle l \rangle$ is independent of Γ_0 .

In a similar manner, we can consider the case where an FM decimation of the partition bond has just occurred at Γ_0 . In this case all the bond strengths just evolve according to independent distributions $P(\beta) = \frac{1}{\Gamma} e^{-\beta/\Gamma}$, so the whole situation is characterized by an overall probabilistic weight w . The RG equation for w is readily derived to be

$$dw = -4w \frac{d\Gamma}{\Gamma}, \quad (59)$$

where the prefactor of 4 is due to the fact that the site containing the partition can be decimated by processes on either side of it which can each be either FM or AFM, thus leading to four possibilities. This equation is solved by $w = (\Gamma/\Gamma_0)^{-4} = e^{-4l}$. The expected value of l at the next decimation is then

$$\langle l \rangle = - \int_0^\infty (de^{-4l}) l = 4 \int_0^\infty e^{-4l} l dl = \frac{1}{4}. \quad (60)$$

Finally, we compute the average $\langle l \rangle$ between AFM decimations, as follows. First, note that there can be any number of FM decimations in between the two AFM decimations. Since each decimation is equally likely to

be AFM and FM, the probability of having precisely k FM decimations is 2^{-k-1} . The expected l is therefore

$$\langle l \rangle = \sum_{n=0}^{\infty} \left(\frac{15}{12} + \frac{1}{4}n \right) 2^{-n-1} = \frac{15}{12} + \frac{1}{4} = \frac{3}{2}. \quad (61)$$

C. Entropy Calculation

We now use the knowledge of mean decimation times to do the entropy calculation. We are interested in the scaling limit of large L , which translates to looking at large $l = \log \frac{L}{\Gamma_0}$. In this case a complicated tree-like structure forms over each endpoint of the length L interval, and we need to figure out its entropy contribution. As we mentioned above, for the case of the random Fibonacci chain with only *AFM* couplings, where the picture is a rainbow diagram straddling each endpoint, the asymptotic contribution in the large rainbow limit of each singlet in the rainbow is $\log_2 \tau$. We will now find an analogous rainbow picture for the mixed Fibonacci chain.

Let us focus on just one boundary of the interval, so we have one partition bond. The ground state trivalent graph that forms over it can be decomposed into connected tree components (fig. 11a) as follows. The first, innermost tree is generated by all the FM decimations prior to the first AFM decimation of the partition bond (if the first decimation is AFM, the tree is just a singlet). The next tree is generated by all the FM decimations between the first and second AFM decimations, and so on. As shown in (fig. 11a) these trees can be thought of as "thickened stripes" - it's just that now the stripes consist of not only a singlet, but an entire tree straddling the partition bond. The idea now is to use F -matrix relations to decompose each tree into a superposition of graphs which have only 0 or 1 τ lines straddling the partition bond, so as to get the ground state to look like a superposition of rainbow diagrams (fig. 11b). The entropy will then be a sum of a rainbow contribution and a contribution coming from the entanglement between the graphs on either side of the partition bond joined by the rainbow stripes.

Before we go into details, let's compute a specific example. Consider the graph in fig. 12, which describes two FM decimations followed by an AFM one. To compute its entanglement entropy we apply the F -matrix move as shown in fig. 12 and decompose it into a superposition of the two graphs on the right side of the equation. The entanglement entropy is then $-\tau^{-2} \log_2(\tau^{-2}) - \tau^{-1} \log_2(\tau^{-1})$. In general we'll need to apply many F -matrix moves and the superposition will be more complicated.

Let's proceed step by step. Label the "thickened stripes" (trees) in fig. 11(a) by an index i , running from 1 to the number of thickened stripes n , and suppose the i th stripe connects a region A_i on the left side of the partition to a region B_i on the right side. Consider Hilbert spaces H_{A_i} and H_{B_i} associated with these

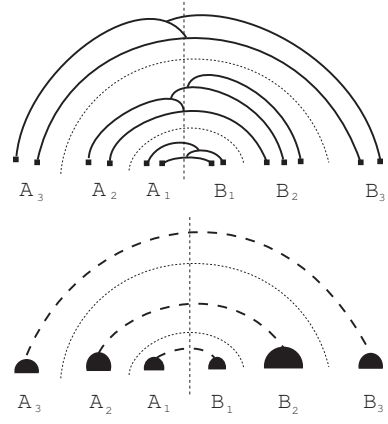


FIG. 11: a) Trivalent graph representing a ground state generated by the real space RG. It can be decomposed into tree components, which are separated by AFM decimations of the partition bond, denoted in the figure by dotted lines. There could also be tree diagrams that don't straddle the partition bond and hence do not contribute to the entanglement entropy; we omit them from the illustration for clarity. b) After applying F -matrix relations we can reduce the trivalent graph in a) to a superposition of graphs of this form. Here the dashed lines denote either a 1 (trivial) or τ (nontrivial) line.

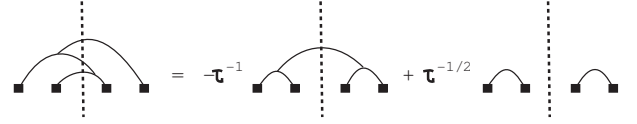


FIG. 12: Application of one F -matrix move decomposes the graph on the left into the superposition on the right.

sites. These are spanned by trivalent graphs having endpoints on those sites, as before, but this time, because the regions may have nontrivial topological charge, we have the familiar decompositions $H_{A_i} = H_{A_i}^0 \oplus H_{A_i}^1$ and $H_{B_i} = H_{B_i}^0 \oplus H_{B_i}^1$. The index 0 and 1 just corresponds to whether or not A_i and B_i are connected by a τ line. The Hilbert Space H_i of the union is

$$H_i = H_{A_i}^0 \otimes H_{B_i}^0 \oplus H_{A_i}^1 \otimes H_{B_i}^1. \quad (62)$$

The ground state is a product state in $H = \bigotimes_i H_i$. Using the decomposition for H_i we write the factors $\psi_i = \alpha_i \psi_i^0 + \beta_i \psi_i^1$. Here ψ_i^j are normalized to have norm 1 and $|\alpha_i|^2 + |\beta_i|^2 = 1$. For convenience we take α_i and β_i real and positive. Let γ be the average over i of $|\beta_i|^2$. When we foil the above product we get the ground state as a superposition of 2^n states with differing rainbow configurations. One can check (by taking inner products and using the no tadpoles rule) that not only are all these states orthogonal, but all the states that enter into the Schmidt decomposition of one (on, say, the left side) are orthogonal to all the states that enter the Schmidt decomposition of the other. This yields a block diagonal decomposition of the density matrix of,

say, the left side. Thus we can deal with the blocks in this block diagonal decomposition separately. We label these 2^n blocks with a label b . Each block b corresponds to a choice of $h_i = 0, 1$, where h_i specifies the topological charge of A_i . The trace of such a block b is

$$t_b = \prod_i \alpha_i^{2h_i} \beta_i^{2(1-h_i)}. \quad (63)$$

Let's compute $-\text{Tr} (M_b \log M_b)$ for block b . To do this we choose a convenient basis for the space where the, say, left components of the Schmidt decomposition of the state corresponding to this graph lie. In general, a basis can be given by the set of all labelings of a trivalent tree, consistent with the fusion rules (i.e., you can't have two 1's and a τ at a vertex). So we pick a tree for each region A_i , and then join these up as in Fig. 13, for a tree defined over the whole left region (note that we're in the subspace where the topological charges of each A_i are fixed by h_i , so we're not looking at *all* labelings, but fixing some of the edges to be τ). This is precisely the kind of graph used in 21 to compute the entropy of the rainbow diagram. The only difference in our case is that we have extra degrees of freedom corresponding to the graphs for each A_i . So we've found a basis which consists of labelings of several subgraphs of a trivalent tree which do not interfere with each other. Namely, these subgraphs are the graphs near each A_i , and an extra one consisting of the edges which link the various A_i - it will lead to the "rainbow" contribution in the equation below. Because there are no *inter*-sub-graph constraints, i.e., the labelings on the sub-graphs can be chosen independently, the entropy is simply a sum of contributions from each subgraph.

$$-\text{Tr} (M_b \log M_b) = -t_b \log t_b + t_b S_b^{\text{rainbow}} + t_b \sum_i S_i^{h_i} \quad (64)$$

Here the first term comes from the normalization of the block b , which has overall trace t_b , the second term is the "rainbow" contribution mentioned above, asymptotically equal to $\log_2 \tau$ times the number of nonzero h_i , and $S_i^{h_i}$ is the entropy associated to ψ_i^j (i.e the contribution from the graphs around A_i and B_i). Summing over all blocks b and performing some elementary algebra, we get the entropy to be

$$S = \sum_i (-2\alpha_i^2 \log \alpha_i - 2\beta_i^2 \log \beta_i + \alpha_i^2 S_i^0 + \beta_i^2 S_i^1) + \langle S_b^{\text{rainbow}} \rangle \quad (65)$$

where the average $\langle S_b^{\text{rainbow}} \rangle$ is taken over all blocks b with weight t_b . This average is approximately equal to $\log_2 \tau$ times the average number of stripes, γn , so that

$$S \sim \sum_i (-2\alpha_i^2 \log \alpha_i - 2\beta_i^2 \log \beta_i + \alpha_i^2 S_i^0 + \beta_i^2 S_i^1) + \gamma n \log_2 \tau \quad (66)$$

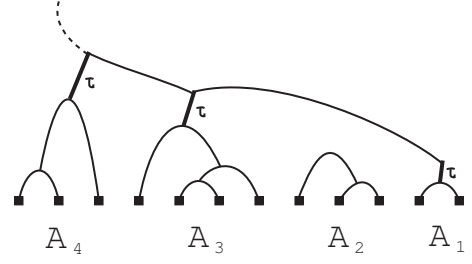


FIG. 13: A trivalent graph whose labelings give a basis for the Hilbert space left of the partition bond. Here we have a tree for each region A_i , with the line leading out of A_i fixed to be τ (for $i = 1, 3, 4$) or 1 (for $i = 2$). The rest of the lines, including the lines connecting different A_i , can be labeled at will, consistent with the fusion rules. The label of the dashed line gives the total topological charge of the left side of the system.

Recall that we defined γ above to be the average over i of $|\beta_i|^2$, which is just the fraction of regions A_i which have non-trivial topological charge.

In eqn. 66 the first quantity sums up the tree contributions S_{tree} discussed at the beginning of this section. Thus eqn. 51 shows that it is equal to

$$\frac{4}{9} < S_{\text{tree}} > \ln L. \quad (67)$$

To compute $\langle S_{\text{tree}} \rangle$ we note that the average is taken over all possible trees generated by FM decimations between two consecutive AFM decimations. There are many possible trees, since we can choose the number r of FM decimations, and for each FM decimation we must decide whether to decimate with the right or the left site. The probability of each such tree is 2^{-2r-1} . We have computed this average numerically via a Mathematica program. The program basically takes each possible tree and builds up the corresponding wavefunction ψ step by step in a convenient basis by applying the FM decimations. It then traces out half the system, finds the eigenvalues of the density matrix, computes the entanglement entropy, and finally averages over the trees. We obtain $\langle S_{\text{tree}} \rangle = 0.115$ approximately. The program also computes $\gamma = 0.927$. Putting this into (66) we get $S = \frac{4}{9} \ln L (0.115 + 0.927 \log_2(\tau))$ so that

$$S = 0.234 \log_2 L. \quad (68)$$

The program goes up to $r = 9$, and we can bound the error obtained by omitting the remaining trees by a quantity exponentially small in r . Basically this is because the probability of having a tree with a given value of r is exponentially small, 2^{r+1} , whereas the maximal entropy contribution of such a tree only scales linearly in n (because the dimension of the Hilbert space is exponential in n). This argument yields a rigorous bound of ± 0.0006 on the coefficient in (68).

Thus the effective central charge we obtain for the

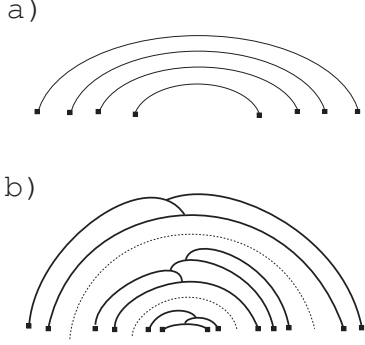


FIG. 14: a) A rainbow diagram. b) Typical state at the FM-AFM point. The dashed lines denote the location of AFM decimations, which separate the “thickened” stripes.

mixed fixed point is:

$$c_{eff}^{mixed} \approx 3 \cdot 0.234 = 0.702. \quad (69)$$

As we will discuss in the conclusion, this result is bigger than the effective charge in the antiferromagnetic random-singlet fixed point.

V. NON-ABELIAN ANYONS AND INFINITE DISORDER

A. Fusion rules and real-space RG

In this paper so far we analyzed the infinite disorder fixed points of the Fibonacci model. Rather surprisingly, the Fibonacci anyons lend themselves very readily to real-space RG analysis, and gives rise to a remarkably rich phase diagram. It is then natural to ask: will similar effects arise in other chains of non-abelian anyons?

In fact, a deep relationship exists between real space RG and the behavior of non-abelian anyons. To see this consider first the ground state of conventional spin chains. In order to find the ground state of a conventional spin chain in a strong-disorder phase, we would apply real-space decimation rules to bond with strong coupling. The type of decimation we apply will depend on the local Hamiltonian and the Hilbert space of the system. For instance, in the spin-1/2 (AFM) Heisenberg model, two neighboring spin-1/2's can fuse according to the the $SU(2)$ rule:

$$\frac{1}{2} \otimes \frac{1}{2} = 0 \oplus 1. \quad (70)$$

A decimation rule applied to these two neighboring spins will choose one of the fusion subspaces - the spin-singlet or spin-triplet - according to the local Hamiltonian. The generalization of this principal to the case of non-abelian chains is nearly trivial. The spin-compounding rule, Eq. (70), is substituted by the *fusion algebra* of the non-

abelian system:

$$a \otimes b = \oplus_c \sum N_{ab}^c c \quad (71)$$

where N_{ab}^c is the number of ways the superselection sectors a and b can fuse into c .

A major difference, however, between rules (70) and (71) is that fusion rules for a non-abelian algebra are always *closed*, while in regular spin-chains, the fusion rules include an infinite set of subspaces. The closure of the fusion rules for non-abelian anyons is a manifestation of the nonlocality of their Hilbert space, and therefore unique to these systems. It implies that one can *always* apply a real-space RG scheme without ever generating new types of coupling in the renormalized Hamiltonian. Furthermore, just as in conventional spin chains, a decimation will result in either in a Ma-Dasgupta renormalization of the neighboring couplings, or in their multiplication by a factor of magnitude smaller than 1. Therefore *sufficiently disordered (and most likely even weakly disordered) non-abelian chains will exhibit an infinite randomness behavior in the large length scale properties of their ground state.*

B. $S > 1/2$ Heisenberg chains and the $SU(2)_k$ fusion algebra

The above observation is easily demonstrated using the mixed FM/AFM fixed point of the Fibonacci anyons. Both FM and AFM couplings between two Fibonacci anyons lead to fusion into either a Fibonacci anyon, or the vacuum:

$$\tau \otimes \tau = \mathbf{1} \oplus \tau. \quad (72)$$

Therefore we can generically carry out a real-space RG analysis to its conclusion. But in spin-1/2 chains with nearest-neighbor couplings that could be either FM or AFM, it is easy to see that we generate higher and higher spins, and as a result do not flow to an infinite randomness fixed point (although a fixed point of the mixed spin-1/2 chain was observed numerically in 24,25), unless their Hamiltonian is restricted, e.g., by a symmetry in the problem which prevents large-moments formation. This is the case in $S > 1/2$ Hiesenberg models^{26–28}, which we will now briefly discuss.

Disordered Heisenberg spin chains with spin $S > 1/2$ were successfully analyzed by a real space decimation procedure that instead of forcing two strongly interacting sites into their lowest energy subspace (usually the singlet), just forbids them from their highest energy subspace, (usually with spin $2S$). This gives rise to sites becoming effectively lower-spin sites, with spins $S_i = 1/2, \dots, S$ ^{26,27}. Although the bare Hamiltonian contains only antiferromagnetic couplings, the decimation procedure also generates ferromagnetic bonds. These raise the spectre of large-spin moment formation, but the bipartiteness of the chain in the bare Hamiltonian guarantees

that these FM coupling can never give rise to a spin larger than the original spin.

The fact that in disordered Heisenberg models the real-space decimation rules only allow the formation of spins no larger than the original spins, makes these rules almost identical to the fusion rules of the truncated $SU(2)$ representations, $SU(2)_k$ with $k = 2S$. As an example consider the spin-1 Heisenberg model. After some renormalization, the spin-1 chain effectively contains sites completely decimated, spin-0, partially decimated, spin-1/2, and sites that are spin-1. Upon real-space decimation, the ground state is formed by the following 'fusion' rules:

$$\begin{aligned} 1 \otimes 1 &= 0 \\ 1 \otimes 1/2 &= 1/2 \\ 1/2 \otimes 1/2 &= 0 \oplus 1 \end{aligned} \quad (73)$$

These fusion channels are picked *energetically*; i.e., two spin-1 sites can fuse into a spin-2 moment, but this will be very costly, and will be excluded from the ground state wave function. The two fusion possibilities of the spin-1/2 in the last line indicate that spin-1/2's can have FM and AFM interactions. If we now compare this to the $SU_2(2)$:

$$\begin{aligned} \epsilon \otimes \epsilon &= \mathbf{1} \\ \epsilon \otimes \sigma &= \sigma \\ \sigma \otimes \sigma &= \mathbf{1} \oplus \epsilon \end{aligned} \quad (74)$$

we can identify the non-trivial superselection sector, σ , with spin-1/2, as expected from the Bratteli diagram, and the trivial sector ϵ with spin-1.

Indeed the two fusion rules are essentially identical. But as opposed to rules (73), which are imposed by energy consideration, the fusion rules (74) are complete, and describe the full Hilbert state, rather than the ground state. Therefore the ground state of a disordered $SU_2(2)$ chain is different than that of a spin-1 disordered Heisenberg chain. In fact, the $SU_2(2)$ reduces to a random Majorana chain, analyzed in Ref. 21, which, has a random singlet ground state. A similar situation prevails in the case of the spin-3/2 Heisenberg model²⁸: the decimation rules for the spin model are almost exactly the same as the fusion rules for $SU_3(2)$ (except for the Heisenberg model *not* allowing the fusion $1 \otimes 1 = 1$, which could be corrected by allowing biquadratic coupling). Nevertheless, the spin-3/2 Heisenberg chain exhibits two random singlet phases, separated by a 4-domain permutation symmetric fixed point, while the behavior of the non-trivial sector of the $SU_3(2)$ is given by the above analysis of the Fibonacci chain.

C. Novel infinite randomness universality classes in non-abelian anyons?

Although the analogy between the spin $S > 1/2$ Heisenberg model decimation rules, and the fusion rules of $SU(2)_k$ theories does not help us find new ground

states, it demonstrates something rather important. Just as the random Heisenberg models allowed the discovery of the permutation symmetric sequence of infinite randomness fixed points¹¹, we expect that an investigation of disordered $SU(2)_k$ chains will also lead to novel infinite randomness universality classes. We leave this study for future research.

D. Limit of $k \rightarrow \infty$

In the case of the disordered AFM golden chain, it is possible to generalize the setup slightly by considering other larger values of k . Retaining the quantum spin 1 representation for the anyons out of which we build the chain, the entire analysis of 21 goes through, with only the quantum dimension changed from τ to $2 \cos(\pi/(k+2))$. It is gratifying to see that in the "classical" limit $k \rightarrow \infty$, we reproduce the spin 1/2 result, with each singlet contributing $\log_2 2 = 1$ to the entanglement entropy.

VI. CONCLUSIONS

In this paper, we carry out an exhaustive analysis of the simplest random chain of non-abelian quasiparticles: the Fibonacci, or golden, chain. Using real-space RG, we are able to analyze the phase diagram and stability of the entire parameter range of the nearest-neighbor Fibonacci chain, where each pair of neighboring sites interacts by assigning an energy cost for fusing in the trivial channel or in the anyonic channel.

The phase diagram we find is split between two phases, both of which are infinite randomness phases. When there are only couplings favoring fusion into the trivial channel (i.e., only AFM couplings) the flow is to the random singlet fixed point. When any finite density of 'ferromagnetic couplings', i.e., couplings preferring the τ fusion channel, are sprinkled in, the random singlet fixed point is destabilized, and the chain flows to a mixed infinite-randomness phase, which is characterized by the energy-length scaling exponent $\psi = \frac{1}{3}$, and a coupling distribution function $\rho(J) \propto \frac{1}{|J|^{1-\chi/\Gamma}}$, with $\chi = 2$, for both FM and AFM cite. This stable fixed point, somewhat surprisingly, is in the same universality class as the transition point between the Haldane phase and the random singlet phase of the random spin-1 Heisenberg model^{11,26,27}. For the golden chain, the mixed fixed point also has a diagrammatic representation in terms of random trivalent graphs. The mixed fixed point is the first non-singlet *stable* infinite randomness fixed point to be discovered.

Another important character of this new IR fixed point is its entanglement entropy. Both infinite randomness fixed points exhibit the characteristic $\log L$ scaling:

$$S = \frac{1}{3} c_{eff}^{mixed} \ln L. \quad (75)$$

The coefficient in front of the \ln for the pure AFM chain was computed in Ref. 21, where it was found that it reflects the quantum dimension of the Fibonacci anyons: $c_{eff}^{RS} = \ln \tau = 0.481$. The entropy scaling in the mixed phase is more intricate owing to the complicated trivalent graph nature of the ground state. We found the effective central charge, c_{eff}^{mixed} , to be:

$$c_{eff}^{mixed} = 3 \cdot 0.234 = 0.702. \quad (76)$$

Since this result was obtained through a combination of numerical and analytical methods, it is hard to gain an intuitive understanding of the numerical result. Nevertheless, it is interesting to compare it to its pure-system analog, and to the effective central charge of the random singlet phase. It is most likely that the mixed IR phase is also the terminus of flow from the ferromagnetic pure fibonacci chain. The central charge of the critical FM golden chains was determined in Ref. 9 to be $c = 4/5 = 0.8 > c_{eff}^{mixed}$. Hence the effective central charge dropped along the flow. Comparing our result, though, to the central charge in the random singlet phase immediately reveals that the effective central charge *increased* in the strong-randomness RG flow from the random singlet phase to the mixed IR phase. Thus the suggestion that strong-randomness flows may have a c-theorem associated with them is contradicted.

This result is rather novel, and it is worth mentioning that one can see that it is true without having to do the full calculation of the entanglement entropy in the mixed FM/AFM phase. To see this, one first of all notices that the average $\langle l \rangle$ between AFM decimations, equal to $3/2$ (eqn. 61), is half of that in the AFM phase. This means the treelike structures form twice as fast as the singlets in the AFM phase. Now, to compare coefficients in front of $\ln L$ one must multiply by the energy length scaling exponent, which is $1/3$ in the mixed phase and $1/2$ in the AFM phase. So the number of treelike structures forming over the endpoints is $4/3$ times the number of singlets in the forming in the AFM phase. However, with probability $1/2$ the treelike structure is simply a singlet (AFM decimation following another AFM decimation), and with probability $1/4$ it is simply a tree on 3 sites (one FM decimation between the AFM decimations), whose contribution to the entropy is the same as a singlets. Thus the treelike structures contribute at least $3/4$ as much entanglement entropy as singlets, and given that there are $4/3$ times as many of them as singlets in the AFM phase, the mixed phase has at least as much entropy as the AFM phase. The fact that the more complicated trees have a nonzero contribution immediately shows that the entropy of the mixed phase is in fact higher than that of the AFM phase.

Now, when we contrast the central charges of the of the two critical phases of the pure chain, $c^{AFM} = 0.7$, and $c^{FM} = 0.8$, we find that by the Zamolodchikov c-theorem,²⁹ the AFM phase must be a stable phase with

respect to the FM one, unless another critical point appears in between, which we speculate is unlikely. On

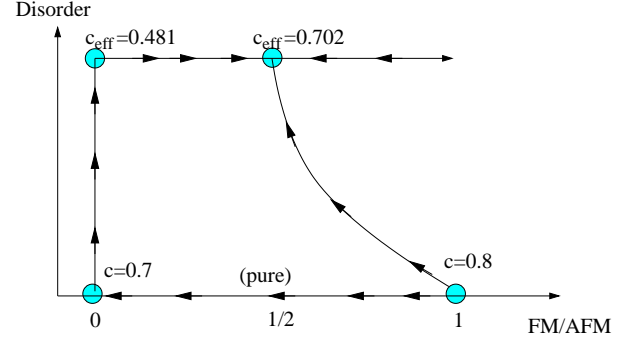


FIG. 15: Flow diagram of the pure and disordered golden chain. In the pure chain, assuming no intervening fixed points exist, the FM fixed point is unstable to flow to the AFM fixed point, as inferred from the Zamolodchikov c-theorem. In the disordered chain, however, the flow is in the opposite direction, with the mixed FM/AFM phase, which is most likely the terminus of the flow from the pure FM phase, being stable relative to the random singlet phase, which is the result of disordering the pure AFM phase. The fixed point (effective) central charges are also quoted.

the other hand, the flow in the random golden chain is the opposite: the mixed FM/AFM phase is stable for essentially all chain coupling distributions, except for the point in which all couplings are antiferromagnetic. This situation is summarized in Fig. 15.

Most importantly, we also observed in this paper the close connection between a fusion algebra and real-space RG. This connection implies that essentially all strongly disordered phases of non-abelian chains will be of the infinite randomness class. In the future we intend to analyze the random phases of non-abelian chains with different fusion algebras. While this research is intended to expand our understanding of random non-abelian systems, it may also lead to the discovery of new infinite-randomness phases and universality classes, beyond the permutation-symmetric sequence of Damle and Huse¹¹.

Acknowledgments

We are indebted to A. Kitaev, J. Preskill, S. Trebst, and P. Bonderson for illuminating discussions. We would like to especially thank K. Yang for his contributions to this project. G.R. and L.F. acknowledge support from NSF Grant No. PHY-0456720. N.E.B. acknowledges support from US DOE Grant No. DE-FG02-97ER45639. J.M. acknowledges support from DMR-0238760. We would also like to acknowledge the KITP, UCSB, for their hospitality.

-
- ¹ F. D. M. Haldane, Phys. Rev. Lett. **50**, 1153 (1983).
 - ² I. Affleck, T. Kennedy, E. H. Lieb, and H. Tasaki, Phys. Rev. Lett. **59**, 799 (1987).
 - ³ D. S. Fisher, Phys. Rev. B **50**, 3799 (1994).
 - ⁴ D. S. Fisher, Phys. Rev. B **51**, 6411 (1995).
 - ⁵ N. Read and D. Green, Phys. Rev. B **61**, 10267 (2000).
 - ⁶ G. Moore and N. Read, Nucl. Phys. B **360**, 362 (1991).
 - ⁷ S. D. Sarma, M. Freedman, and C. Nayak, Phys. Rev. Lett. **94**, 166802 (2005).
 - ⁸ M. H. Freedman, A. Kitaev, M. J. Larsen, and Z. Wang, *Topological quantum computation*, quant-ph/0101025.
 - ⁹ A. Feiguin, S. Trebst, A. W. W. Ludwig, M. Troyer, A. Kitaev, Z. Wang, and M. H. Freedman, Phys. Rev. Lett. **98**, 160409 (2007).
 - ¹⁰ S. Trebst, E. Ardonne, A. Feiguin, D. A. Huse, A. W. W. Ludwig, and M. Troyer, *Collective states of interacting fibonacci anyons*, arXiv:0801.4602.
 - ¹¹ K. Damle and D. A. Huse, Phys. Rev. Lett. **89**, 277203 (2002).
 - ¹² F. Igloi and C. Monthus, Phys. Rep. **412**, 277 (2005).
 - ¹³ J. A. Hoyos and E. Miranda, Phys. Rev. B **70**, 180401 (2004).
 - ¹⁴ C. Holzhey, F. Larsen, and F. Wilczek, Nucl. Phys. B **424**, 44 (1994).
 - ¹⁵ P. Calabrese and J. Cardy, J. Stat. Mech. **06**, P06002 (2004).
 - ¹⁶ G. Vidal, J. I. Latorre, E. Rico, and A. Kitaev, Phys. Rev. Lett. **90**, 227902 (2003).
 - ¹⁷ G. Refael and J. E. Moore, Phys. Rev. Lett. **93**, 260602 (2004).
 - ¹⁸ G. Refael and J. E. Moore, Phys. Rev. B **76**, 024419 (2007).
 - ¹⁹ N. Laflorencie, Phys. Rev. B **72**, 140408 (2005).
 - ²⁰ R. Santachiara, J.Stat. Mech. p. L06002 (2006).
 - ²¹ N. E. Bonesteel and K. Yang, *Infinite-randomness fixed points for chains of non-abelian quasiparticles* (2007).
 - ²² S. K. Ma, C. Dasgupta, and C. K. Hu, Phys. Rev. Lett. **43**, 1434 (1979).
 - ²³ C. Dasgupta and S. K. Ma, Phys. Rev. B **22**, 1305 (1980).
 - ²⁴ A. Furusaki, M. Sigrist, P. A. Lee, K. Tanaka, and N. Nagaosa, Phys. Rev. Lett. **73**, 2622 (1994).
 - ²⁵ A. Furusaki, M. Sigrist, E. Westerberg, P. A. Lee, K. B. Tanaka, and N. Nagaosa, Phys. Rev. B **52**, 15930 (1995).
 - ²⁶ C. Monthus, O. Golinnelli, and T. Jolicœur, Phys. Rev. B **58**, 805 (1998).
 - ²⁷ R. A. Hyman and K. Yang, Phys. Rev. Lett. **78**, 1783 (1997).
 - ²⁸ G. Refael, S. Kehrein, and D. S. Fisher, Phys. Rev. B **66**, 060402 (2002).
 - ²⁹ A. B. Zamolodchikov, JETP Lett. **43**, 730 (1986).